PASJ: Publ. Astron. Soc. Japan **59**, S543–S555, 2007 October 10

Optical Identification of 15 μm Sources in the AKARI Performance Verification Field toward the North Ecliptic Pole

Hideo MATSUHARA,[1] Takehiko WADA,[1] Chris P. PEARSON,[1,10] Shinki OYABU,[1] Myungshin IM,[2] Koji IMAI,[1] Toshinobu TAKAGI,[1] Eugene KANG,[2] Narae HWANG,[2] Woong-Seob JEONG, [1] Hyung Mok LEE,[2] Myung Gyoon LEE,[2] Soojong PAK,[3] Stephen SERJEANT,[4] Takao NAKAGAWA,[1] Hitoshi HANAMI,[5] Hanae INAMI,[11] Takashi ONAKA,[6] Naofumi FUJISHIRO,[1*] Daisuke ISHIHARA,[6] Yoshifusa ITA,[1] Hirokazu KATAZA,[1] Woojung KIM,[1] Toshio MATSUMOTO,[1] Hiroshi MURAKAMI,[1] Youichi OHYAMA,[1] Itsuki SAKON,[6] Toshihiko TANABÉ,[7] Kazunori UEMIZU,[1] Munetaka UENO,[8] and Hidenori WATARAI[9]

[1]*Institute of Space and Astronautical Science, Japan Aerospace Exploration Agency, 3-1-1 Yoshinodai, Sagamihara, Kanagawa 229-8510*
maruma@ir.isas.jaxa.jp
[2]*Department of Physics & Astronomy, FPRD, Seoul National University, Shillim-Dong, Kwanak-Gu, Seoul 151-742, Korea*
[3]*Kyung Hee University, 1 Seocheon-dong, Giheung-gu, Yongin-si Gyeonggi-do 446-701, Korea*
[4]*Department of Physics and Astronomy, The Open University, Milton Keynes, MK7 6AA, UK*
[5]*Iwate University, 3-18-8 Ueda, Morioka 020-8550*
[6]*Department of Astronomy, School of Science, The University of Tokyo, 7-3-1 Hongo, Bunkyo-ku, Tokyo 113-0033*
[7]*Institute of Astronomy, The University of Tokyo, 2-21-1 Osawa, Mitaka, Tokyo 181-0015*
[8]*Department of Earth Science and Astronomy, Graduate School of Arts and Sciences, The University of Tokyo, 3-8-1 Komaba, Meguro, Tokyo 153-8902*
[9]*Office of Space Applications, Japan Aerospace Exploration Agency, Tsukuba, Ibaraki 305-8505*
[10]*ISO Data Centre, ESA, Villafranca del Castillo, Madrid, Spain*
[11]*Department of Space and Astronautical Science, The Graduate University for Advanced Studies, 3-1-1 Yoshinodai, Sagamihara, Kanagawa 229-8510*

(Received 2007 May 27; accepted 2007 August 20)

Abstract

We present the results of optical identifications for 257 mid-infrared sources detected with a deep 15 μm survey over approximately 80 arcmin^2 area in the AKARI performance verification field near the North Ecliptic Pole. The 15 μm fluxes of the sources range from 1 mJy down to 40 μJy, approximately one half of which are below 100 μJy. Optical counterparts were searched for within a 2″–3″ radius in both the $BVRi'z'$ catalog generated by using the deep Subaru/Suprime-cam field, which covers one-third of the performance verification field, and the $g'r'i'z'$ catalog based on observations made with MegaCam at CFHT. We found that the $B-R$ and $R-z'$ colors of sources with successful optical identifications are systematically redder than that of the entire optical sample in the same field. Moreover, approximately 40% of the 15 μm sources show colors with $R-L15 > 5$, which cannot be explained by the spectral energy distribution (SED) of normal quiescent spiral galaxies, but are consistent with SEDs of redshifted ($z > 1$) starburst or ultraluminous infrared galaxies. This result indicates that the fraction of the ultraluminous infrared galaxies in our faint 15 μm sample is much larger than that in our brighter 15 μm sources, which is consistent with the evolving mid-infrared luminosity function derived by recent studies based on Spitzer 24 μm deep surveys. Based on an SED fitting technique, the nature of the faint 15 μm sources is further discussed for a selected number of sources with available K_s-band data.

Key words: galaxies: evolution — galaxies: statistics — infrared galaxies — space vehicles: instruments

1. Introduction

Finding new populations of faint high-redshift galaxies is an important step to unveil the Cosmic star-formation history of the Universe. Deep mid-infrared (especially at 15 μm) and far-infrared (at 90, 170 μm) surveys with the Infrared Space Observatory (ISO, Genzel & Cesarsky 2000, and references therein) discovered a distinct population with faint optical fluxes and large infrared luminosities ($L_{\rm bol} \geq 10^{11} L_{\odot}$, Elbaz et al. 2002) at $z \geq 0.5$. The 15 μm source counts obtained with the ISO surveys implied strong evolution in the galaxy population (Genzel & Cesarsky 2000; Aussel et al. 1999; Serjeant et al. 2000; Gruppioni et al. 2002; Oliver et al. 2002). Not only the source count models for mid-IR counts, but also the X-ray data (Manners et al. 2004) and subsequent spectroscopic studies (Rowan-Robinson et al. 2004) confirmed that the bulk of the ISO sources were starburst galaxies not AGNs.

The Spitzer Space Telescope (Werner et al. 2004) also offers excellent sensitivities in the four IRAC wavebands between 3.6

* Present address : Cybernet systems Co. Ltd., Bunkyo-ku, Tokyo 112-0012.

and 8.0 μm (Fazio et al. 2004) and at MIPS 24 μm (Rieke et al. 2004), and has revealed that the key epoch to understand the formation and evolution of massive ($M \geq 10^{11} M_{\odot}$) galaxies is at $z = 1$–2; the star formation activity of massive galaxies at $z \sim 2$ is one hundred-times larger than that at present (Chary 2006; Caputi et al. 2006). These ultra-luminous ($L \geq 10^{12} L_{\odot}$) infrared galaxies (ULIRGs) may be progenitors of present-day massive galaxies. In order to reveal their nature, we require complete, uniform samples of massive star-forming galaxies at $z = 1$–2. Although the Spitzer 24 μm deep surveys can probe galaxies at this redshift range, deep surveys at shorter mid-infrared wavelengths (10–20 μm, in the gap between the IRAC 8 μm band and the MIPS 24 μm band) are very important to unveil their nature, since the strong 6.2 and 7.7 μm PAH features prominent in the mid-infrared spectra of star-forming galaxies can enter the MIPS 24 μm passband only at $z > 2$. Spitzer/IRS (Houck et al. 2004) has an imaging capability at 16 μm via its peak-up camera; with this camera deep 16 μm surveys over 150 arcmin^2 in each of GOODS-North and GOODS-South fields have been carried out to depths of 50–85 μJy (3σ) (Teplitz et al. 2005; Teplitz et al. 2006). However, the areal coverage is not yet comparable to the surveys at 24 μm due to the relatively small field of view 1.2 arcmin^2 of the IRS peak-up camera.

The AKARI satellite, launched on 2006 February 21 (UT), has a capability for deep mid-infrared imaging in the Spitzer wavelength desert between 8 μm and 24 μm through one of its focal-plane instruments, the InfraRed Camera (IRC, Onaka et al. 2007). The IRC incorporates three infrared cameras covering nine bands between 2 and 24 μm suitable for deep cosmological surveys. Note that due to the nature of the orbit of AKARI (Sun-synchronous), the visibility of any point on the sky is a strong function of the ecliptic latitude and thus deep surveys are only possible at the ecliptic poles. The AKARI North Ecliptic Pole (NEP) survey is a major legacy of the AKARI mission, consisting of a deep 0.4 square degree and shallow 6.2 square degree survey in all 9 IRC bands (Matsuhara et al. 2006). The AKARI NEP surveys, especially at 11, 15, and 18 μm, are well matched to the Spitzer 24 μm surveys (e.g., Papovich et al. 2004), sampling similar cosmological volumes, and are more sensitive to high redshift star-formation activity than the shorter wavelength Spitzer/IRAC 8 μm band.

In this paper we describe a selection of initial results from the deep extragalactic survey around the NEP region, while focusing on the optical nature of the faint 15 μm sources detected in the performance verification phase of the AKARI mission. The 15 μm sample is especially unique, since more than 100 sources are fainter than 100 μJy, a limit below that obtained with ISO. In section 2, we briefly describe the AKARI data as well as the optical data obtained with Subaru/Suprime-cam and CFHT/Megacam, and identification results of the optical counterparts. In section 3, we discuss the nature of the 15 μm sample based on the optical–mid-infrared colors. Section 4 gives a summary of the paper. Throughout the paper we use the AB maginitude system, unless otherwise explicitly noted; 20 AB magnitude correspond to 36 μJy. We adopt a cosmology of $\Omega_m = 0.3$, $\Omega_\Lambda = 0.7$, and $H_0 = 70\,\mathrm{km\,s^{-1}\,Mpc^{-1}}$.

2. The Data and the Results of Identification

2.1. AKARI/IRC Mid-Infrared Data

The NEP deep survey is centred on a circle at RA = $17^{\mathrm{h}}55^{\mathrm{m}}24^{\mathrm{s}}$, Dec = $+66^{\circ}37'32''$. However, during the performance-verification phase (2006 April 13–May 8) of the AKARI mission, a pilot survey of the NEP over a single field of view of the IRC (approximately $10'\times10'$, hereafter referred to as the performance verification field) at RA = $17^{\mathrm{h}}57^{\mathrm{m}}.3$, Dec = $+66^{\circ}54'.3$, ten pointings deep in the IRC *L15* band (i.e., in the 15 μm band) was carried out.

Here we briefly report on observations and the data reduction; full details are described in Wada et al. (2007). The data for this work were taken using the IRC05 Astronomical Observation Template (AOT) mode, which is optimized for deep survey observations. Note that the IRC05 AOT minimizes overheads by using the minimum number of resets, no filter change and moreover no dithering operation during the 10-minute integration time for one pointing. Therefore, the dithering is performed among the individual pointing observations to remove the effects of dead/hot pixels and cosmic rays, etc. The total net exposure time of the ten pointing observations was 4417 seconds. The data from individual frames for each pointing were reduced using the standard IRC data-reduction pipeline version 060801[1] within the IRAF environment.[2] The IRC pipeline splits pointings into individual frames and corrects for instrument characteristics by masking anomalous/dead pixels, and then applies dark subtraction, a linearity correction, saturation, a distortion correction, and flat fielding, etc. Astrometric data (world coordinate system, WCS) is applied by matching bright stars within the data with 2MASS counterparts. Identification of bright point sources in the deep optical image (T. Wada et al. 2007 in preparation, see subsection 2.2) by eye suggests that the positional accuracy of the WCS is much better than two pixels ($5''$). The resulting stacked images for the individual pointing observations are then co-added by identifying the relatively bright sources in each processed image of one pointing. Finally, the edge of the image, where the signal-to-noise ratio is worse, was trimmed, resulting in a final image size of 77.29 arcmin^2. We used SExtracter (Bertin & Arnouts 1996) for source detection, and source fluxes were evaluated by aperture photometry with a radius of $1''.3$. In total, 257 sources were extracted between *L15* = 16 and 20 magnitudes, of which 110 sources were fainter than 19 mag.

At present, the depth of the final *L15* image is approximately 42 μJy in 3σ, probably due to the fact that the source-extraction technique is not yet optimized. The completeness analysis result implies that the number of sources below 150 μJy is substantially underestimated, but, once detected, the source detection is reliable down to *L15* = 20 mag (or 36 μJy; Wada et al. 2007). This is justified since 60–80% of the sources fainter than *L15* = 18 mag can be identified in the optical

[1] AKARI IRC Data Users Manual ⟨http://www.ir.isas.jaxa.jp/ASTRO-F/Observation/#IDUM⟩.

[2] IRAF is distributed by the National Optical Astronomy Observatory, which is operated by the Association of Universities for Research in Astronomy, Inc., under cooperative agreement with the National Science Foundation.

Table 1. Summary of identifications in the Subaru image (2″ search radius).

15 μm magnitude	Number of total 15 μm sources	Number of sources inside the Subaru image	Number of sources with successful identification
16–18	44	18	15(0)*
18–19	103	40	33(2)
19–20	110	47	32(7)

* All 18 sources have conterparts within 3″ search radius. Numbers in the parentheses are those with two or more optical counterparts.

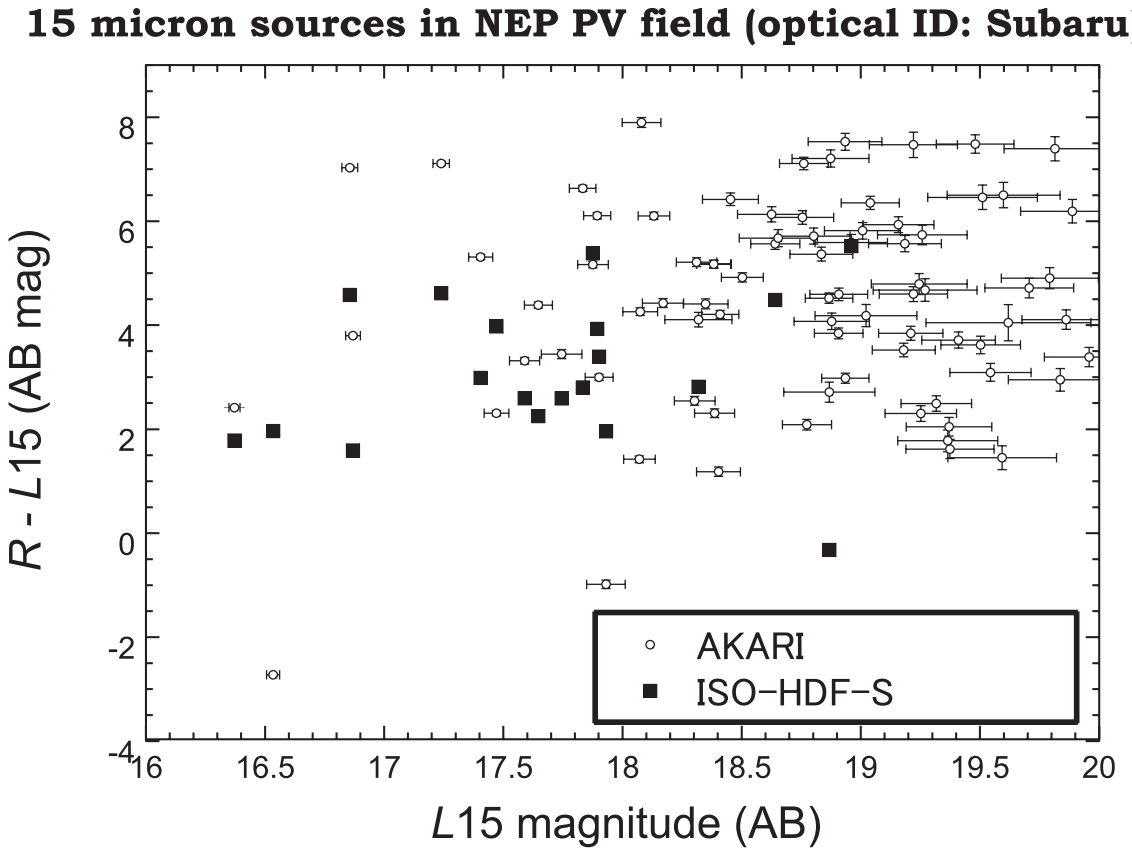

Fig. 1. Observed optical – mid-infrared color vs 15μm magnitude (AB) for all 15 μm sources with successful identification on the Subaru/Suprime-cam source catalog. Black squares represent the HDF-S sources detected with the ISOCAM LW3 15 μm deep survey (Oliver et al. 2002; Mann et al. 2002).

images (see subsection 2.3).

2.2. *Optical Data*

Approximately one third of the performance verification field is covered by a single Subaru Suprime-cam field of view (916 arcmin^2) to $B = 28.4$, $V = 27$, $R = 27.4$, $i' = 27$, $z' = 26.2$ (3σ, AB magnitude, T. Wada et al. 2007, in preparation). The observations were carried out in 2003 June and September with a typical seeing of 1.″0.

The remaining two thirds of the performance verification field is covered by g', r', i', z'-band images taken with the MegaCam instrument on the Canada–France–Hawaii Telescope (CFHT). The MegaCam observation was carried out in 2004 August/September to support the AKARI NEP survey. The observed field covers roughly a 2° by 1° field of view centered on the NEP; therefore, the whole performance verification field is covered by the CFHT imaging data. The depth of the CFHT image is estimated to be $g' \sim 26.4$ mag, $r' \sim 25.9$ mag, $i' \sim 25.3$ mag, and $z' \sim 24.0$ mag at 3σ over an aperture with 1.″0 diameter, but effectively the source counts are complete only down to a limit of about 1.5 magnitudes brighter than the above numbers. The absolute astrometric accuracy of the CFHT mosaic data was measured to be about r.m.s $\sim 0.''4$. More details on the CFHT images can be found in Hwang et al. (2007).

2.3. *Identification with Subaru/Suprime-Cam Source Catalog*

The result of the identification within a 2″ search radius is shown in table 1. Due to the partial coverage of the Subaru image, only 105 sources are inside the Subaru image. Between

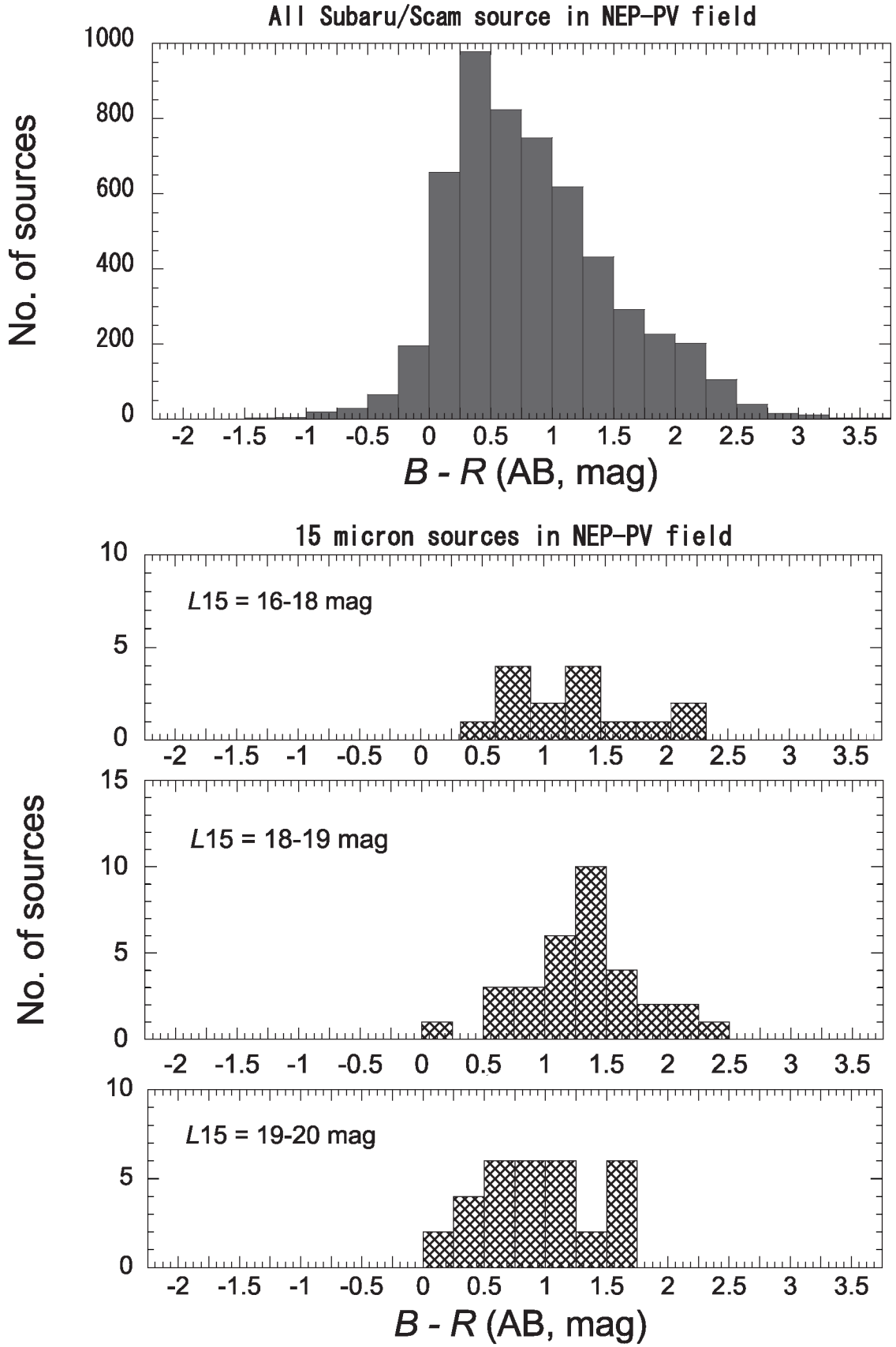

Fig. 2. Observed optical ($B - R$) color for all z'-band selected Subaru/Suprime-cam source catalog in the field (top) and for the 15 μm sources with successful identification on the Subaru/Suprime-cam source catalog (bottom).

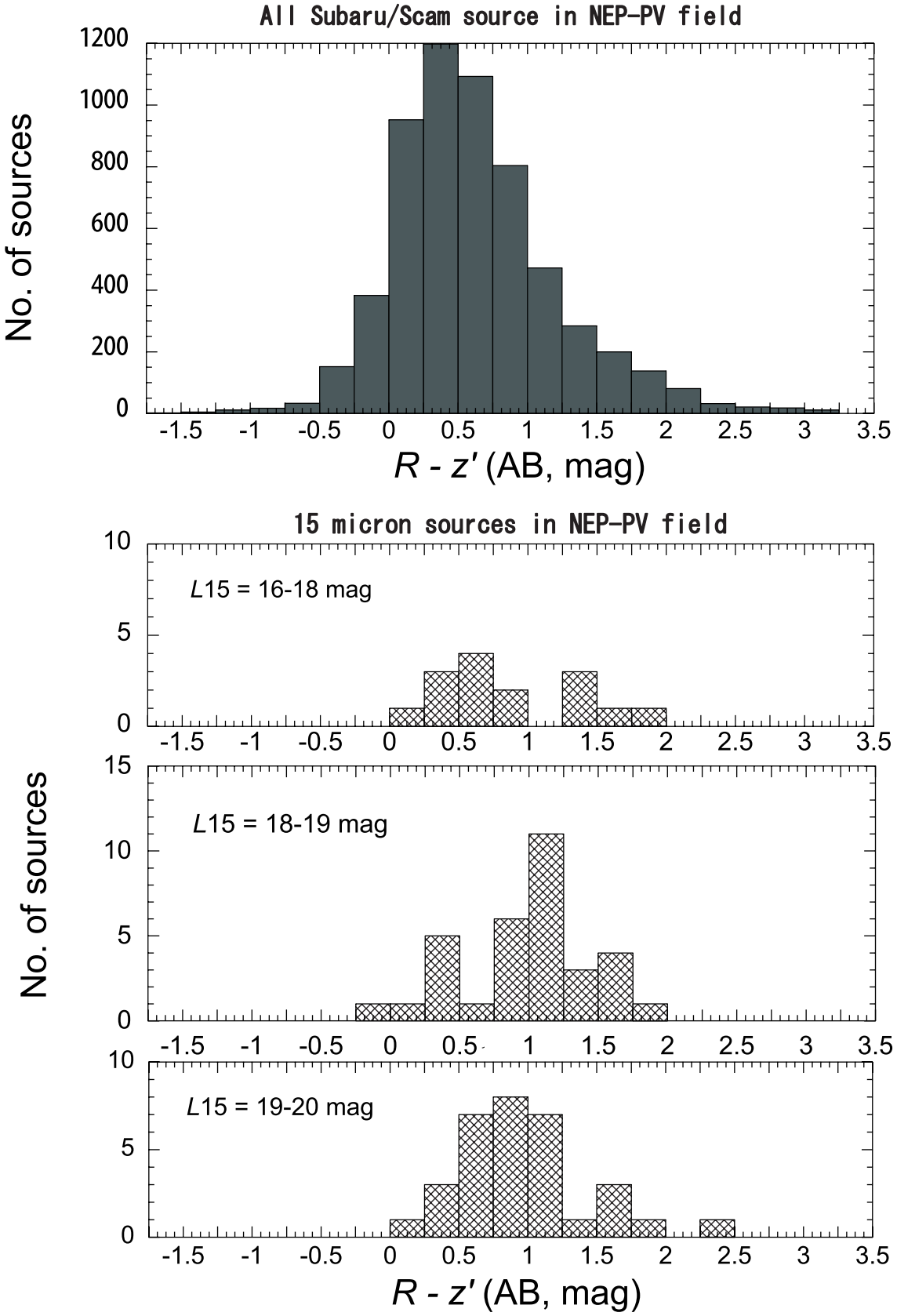

Fig. 3. Observed optical ($R - z'$) color for all z'-band selected Subaru/Suprime-cam source catalog in the field (top) and for the 15 μm sources with successful identification on the Subaru/Suprime-cam source catalog (bottom).

Table 2. Summary of identifications in the CFHT image.*

15 μm magnitude	Number of sources inside the CFHT image	Number of sources in 3 search radius	Number of sources in 2″ search radius
16–18	42	39(13)	27(3)
18–19	99	61(10)	50(5)
19–20	108	67(7)	49(4)

* Numbers in parentheses are those with two or more optical counterparts.

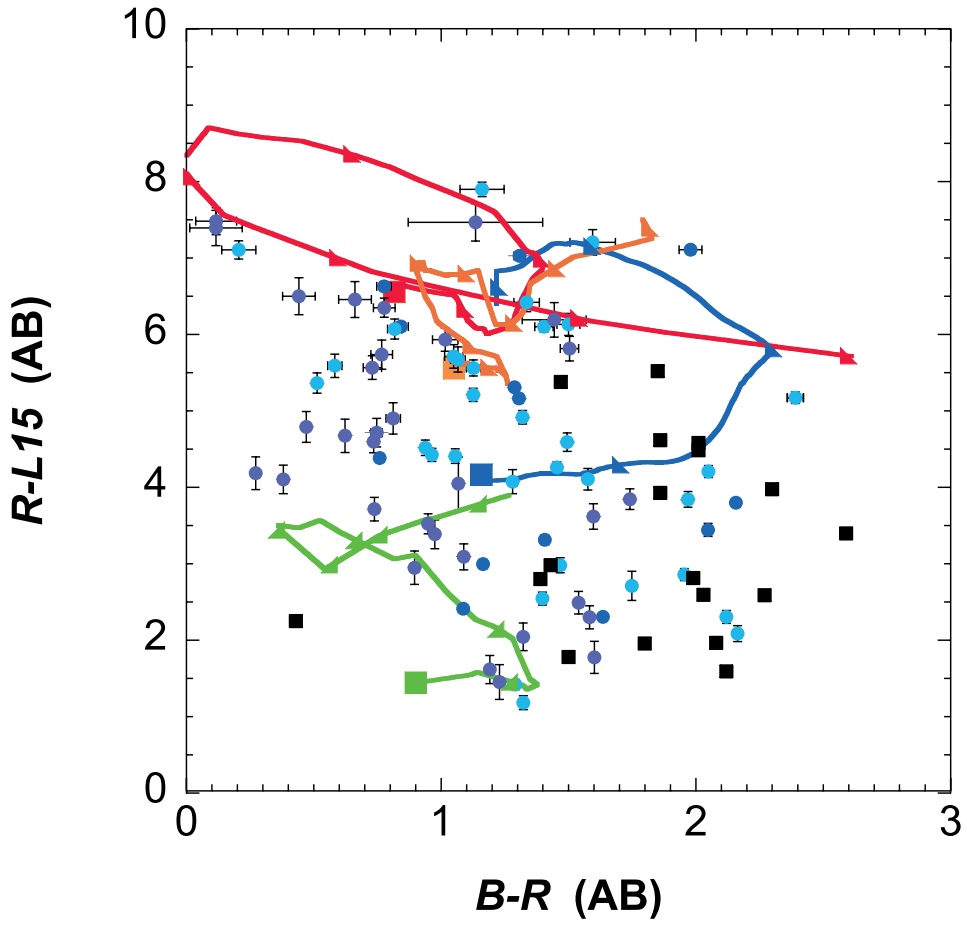

Fig. 4. $B-R$ vs $R-L15$ plot for the 15 μm sources with successful identifications in the Subaru/Suprime-cam source catalog. Dark-blue, light-blue, and purple, circles represent the 16–18, 18–19, 19–20 AKARI 15μm AB magnitudes respectively. Color–color tracks for 4 SED templates are presented. Black squares represent the HDF-S sources detected with the ISOCAM LW3 deep survey (Oliver et al. 2002; Mann et al. 2002). Green, a normal quiescent spiral galaxy (M 51 template); blue, a star-forming galaxy (M 82 template); red, an ultraluminous infrared galaxy (ULIRG) Arp 220 template; orange, an ULIRG, HR 10 template. The large colored squares are the zero redshift points for the SED templates and the markers along the template color tracks represents steps of 0.5 in redshift.

L15 = 16 and 18 magnitudes, all three *L15* sources without optical matches are found to be a blend of several sources, or a part of a large, bright galaxy. The blend of several sources in *L15* causes the coordinates to be calculated as the mean of the multiple sources, making it escape from the 2″ matching radius. Between *L15* = 18 and 19 magnitudes, six out of seven *L15* sources without optical matches are found to be a part of a bright optical counterpart, or located near the edge, or a blend of multiple sources. The remaining source is found near the edge of the *L15* image. It could be a genuine mid-infrared source with no optical counterpart, but it is located near the edge of the *L15* image where the signal-to-noise ratio is low. Between *L15* = 19 and 20 magnitudes, 12 souces out of 15 with no optical counterpart are again, blend of multiple sources, inside optically bright galaxies, or probably spurious objects near the edge of the *L15* image. The remaining three *L15* sources may be genuine optically faint sources. Overall, of 24 *L15* sources without optical matches, only three or four are found to be sources without optical counterparts, which are worth being carefully investigated by multi-color images taken

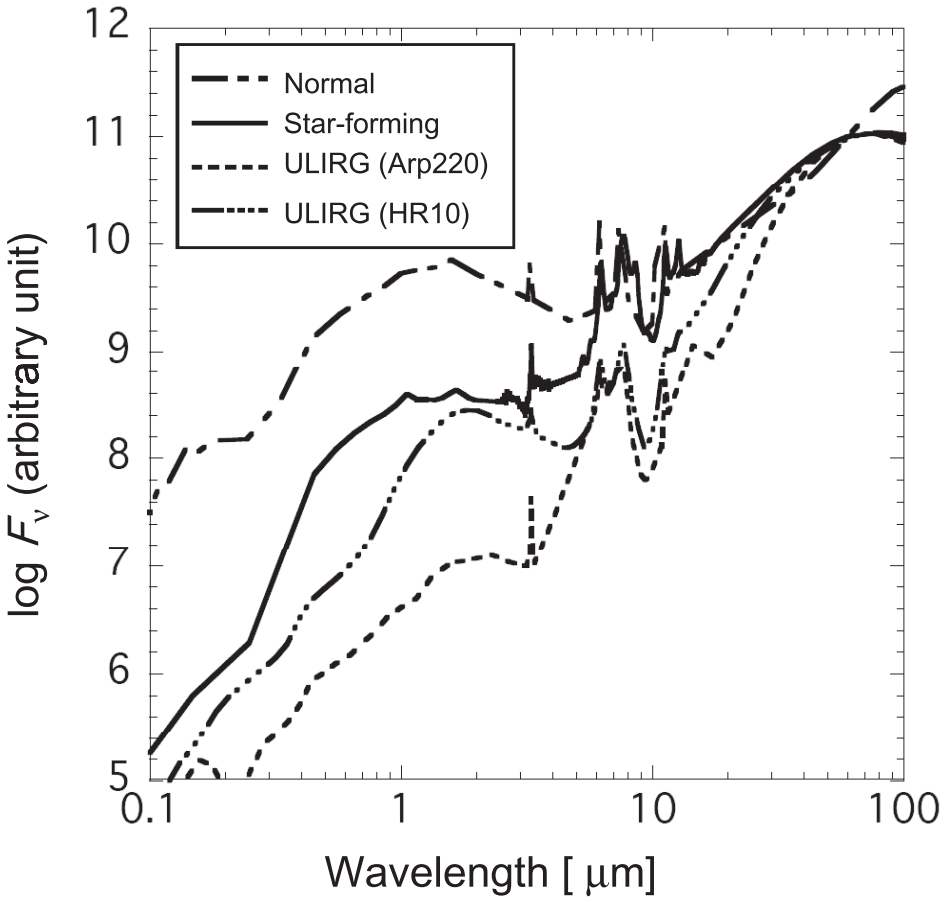

Fig. 5. Rest-frame optical to far-infrared spectral energy distribution templates for: dashed line, a normal quiescent spiral galaxy (M 51 template); solid line, a star-forming galaxy (M 82 template); dotted line, an ultraluminous infrared galaxy (ULIRG), Arp 220 template; dash-dash-dot-dot, an ULIRG, HR 10 template. Model templates are taken from Efstathiou and Rowan-Robinson (2003) for the normal galaxy template, Efstathiou et al. (2000) for the star-forming and Arp 220 templates and Takagi et al. (2003b) for the HR 10 template.

during the NEP survey program. The rest are *L15* detection of multiple sources, sources within optically bright galaxies, or erroneous matches near the edges.

Figure 1 shows their $R-L15$ color with 15 μm magnitude. Except for the very blue sources, which are found to be bright stars (point-like sources in the Subaru image), the $R-L15$ color distribution does not change with 15 μm magnitude, and has a median value of $R-L15 = 4.6$ mag.

As examples showing their optical color characteristics, in figures 2 and 3 we show a comparison of the $B-R$, $R-z'$ colors between all the Subaru sources in the NEP performance verification field and the 15 μm sources. The optical colors of the 15 μm sources show a clear trend towards a redder color: 0.3–0.4 mag redder in $B-R$, and 0.2–0.5 mag in $R-z'$. This indicates that the 15 μm sources sample either a relatively high-redshift population or a population exhibiting dust reddening. Moreover, the fainter 15 μm sources at or below 18 mag (AB) show a redder $R-z'$ color (approximately 0.3 mag) than the brigher sources. This may indicate that fainter 15 μm sources are at relatively high redshift, since the shift of their Balmer/4000A spectral break in between the R and z' bands will create redder $R-z'$ colors.

2.4. Identification with CFHT/Megacam Source Catalog

The result of a cross-identification with a 2″ search radius for optical sources in the CFHT images is shown in table 2.

We find optical counterparts for 93% of the bright *L15* sources ($16 < L15 < 18$ mag), which is consistent with the matching result using the Subaru data. A large fraction of sources with a positional offset of between 2″ and 3″ turn out to be multiple optical sources blended into a single object in the *L15* image. For fainter *L15* sources, the matching probability drops to $\sim$ 65% with a 3″ matching radius and down to 50% when we use a 2″ matching radius. The above number is about 10–30% less than the matching probability of 60–80% for *L15* sources in the Subaru image. The discrepancy mainly comes from the fact that about 10% of *L15* sources have optical magnitudes of around $R \sim 26$ (figure 1), for which no r'-band counterparts are found in the CFHT image. Thus, although the CFHT image covers the entire performance verification field, we only use the sources in the Subaru image for discussing the nature of the faint 15 μm sources.

One should note that the simple automatic identification presented here also suffers from a chance coincidence. Based on the number counts of r'-band sources presented in Hwang

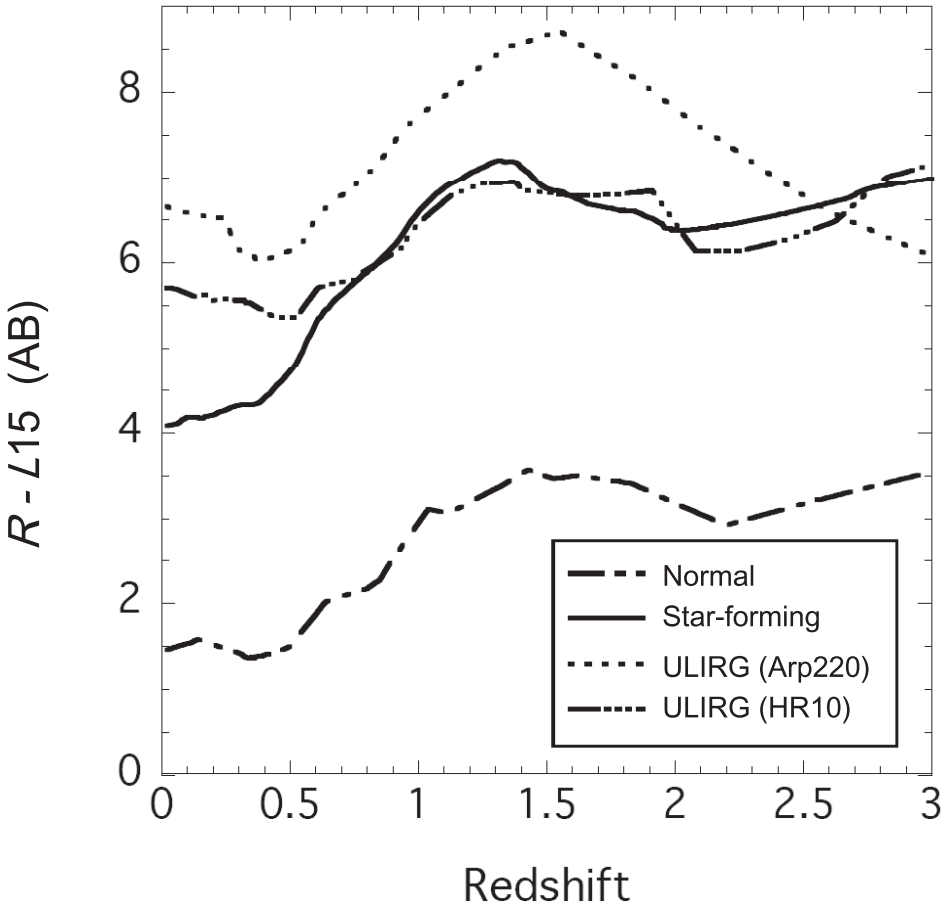

Fig. 6. Optical to mid-infrared $R-L15$ color vs redshift for various template SEDs shown in figure 5. The SEDs were convolved with the filter-band response curves, and then the color was derived.

et al. (2007), the chance coincidence of source identification is 6% and 15% for a 3″ search radius for sources at $r' < 22$ and $r' < 24$, respectively. This number drops to 3% and 7% for a 2″ search radius. Clearly, the 2″ search radius suffers much less from chance coincidence. However, a 2″ radius may be too small in the case for some 15 μm sources where the mid-infrared flux originates from multiple sources.

2.5. *Identification with KPNO/Flamingos Near-Infrared Source Catalog*

The Subaru/Suprime-cam field around the NEP is also covered by the KPNO 2.1m/FLAMINGOS at the J and K_s bands to a depth of $J = 21.6$ and $K_s = 19.9$ (3σ) in Vega magnitudes ("Field-NE" in Imai et al. 2007). Thus we also searched for near-infrared counterparts of the 15 μm sources with optical identifications in the Subaru/Suprime-cam images. However, the performance verification field is located at the edge of the survey field, and thus the number of available images for stacking varies within the image, and also additionally suffers from image distortion from the FLAMINGOS camera. As a result, among the total 81 sources listed in table 1, only 27 and 28 are identified in the J and K_s bands, respectively, with 23 sources being identified in both the J and K_s bands. Since the near-infrared data is incomplete, we only utilized the near-infrared magnitudes for investigating several selected sources with relatively reliable identifications (see subsection 3.2).

3. Discussion

3.1. *Colors of the AKARI 15μm Population*

In figure 4 we plot the $B-R$ vs $R-L15$ colors of the AKARI 15μm sources with successful identifications in the Subaru/Suprime-cam source catalog. The AKARI 15μm populations are plotted over 3 magnitude ranges (15μm AB) from 16–18, 18–19, and 19–20 magnitude. The AKARI population spans a broad range in $R-L15$ colors from $R-L15 = 1$ to 8. To investigate the colors of the AKARI 15μm population we introduced a set of archetypal galaxy spectral energy distribution (SED) templates. These templates are shown in figure 5, and comprise a normal quiescent spiral galaxy modeled on the SED of M 51, a dusty star-forming galaxy modeled on the SED of M 82, and ULIRGs modeled on the SEDs of Arp 220 and HR 10. The normal galaxy template is taken from the radiative transfer models of Efstathiou and Rowan-Robinson (2003) and the star-forming galaxy and ULIRG (Arp 220) templates are taken from the radiative transfer models of Efstathiou et al. (2000). We also include another ULIRG template modeled on the SED of HR 10 (Graham & Dey 1996) using the starburst spectral template

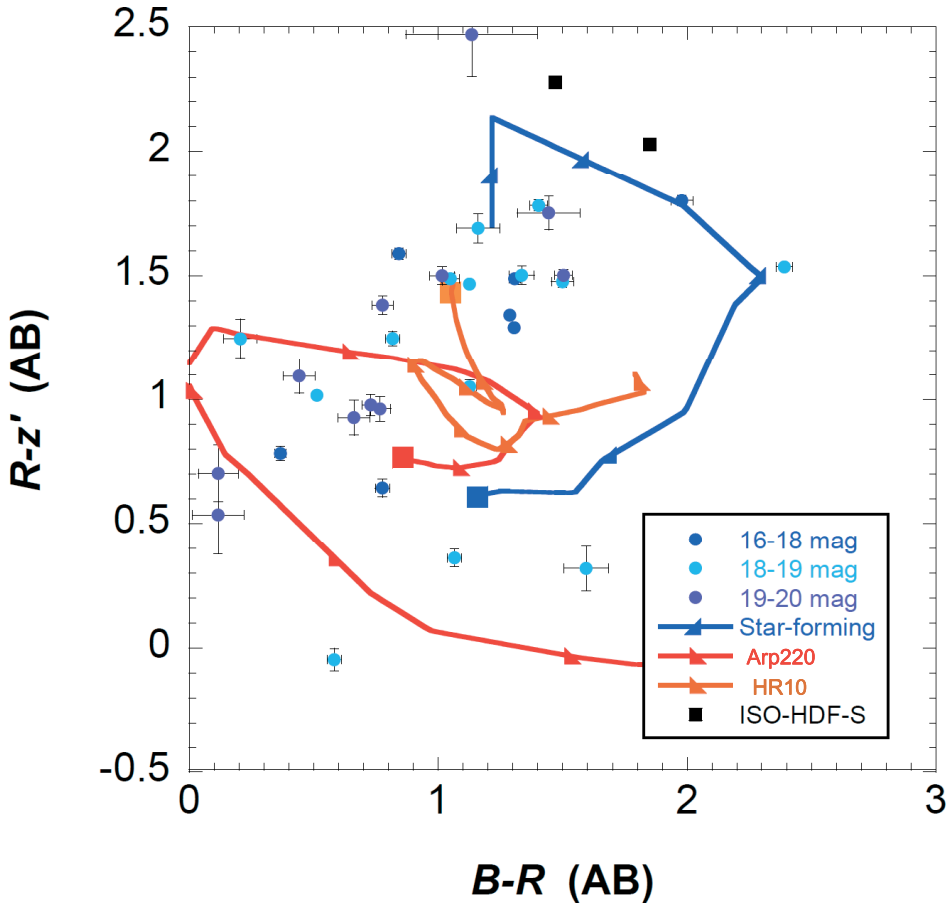

Fig. 7. $B-R$ vs $R-z'$ plot for the 15 μm sources with $R-L15>5$ in the Subaru/Suprime-cam source catalog. Dark-blue, light-blue, and purple, circles represent 16–18, 18–19, 19–20 AKARI 15 μm AB magnitudes, respectively. Two black squares represent the HDF-S sources (Oliver et al. 2002;Mann et al. 2002). Color–color tracks for 3 SED templates are presented: blue, a star-forming galaxy (M 82 template); red, an ultraluminous infrared galaxy (ULIRG), Arp 220 template; orange, an ULIRG, HR 10 template. The large colored squares are the zero redshift points for the SED templates and the markers along the template color tracks represents steps of 0.5 in redshift.

library of Takagi et al. (2003a, 2003b). HR 10 at $z=1.44$ is one of famous Extremely Red Objects (EROs) and its best-fitting SED model is characterized by an older age and larger stellar mass than those of Arp 220 (Takagi et al. 2003b). In figure 6, we plot the $R-L15$ color of our model templates smoothed by the AKARI IRC filter-band response curves as a function of redshift. In general for any redshift, the dusty infrared sources are well separated from the normal quiescent galaxies, consistently having $R-L15>4$. Figure 6 also suggests that sources with $R-L15>6$ or 7 may be plausible candidates for redder dusty star-forming galaxies and ULIRGs, respectively, at $1<z<2$. Since at $z=1$–2 the PAH emission features at 6.2 and 7.7 μm from the star-forming galaxies enter the $L15$ passband, and thus the $R-L15$ color become redder, these red $R-L15$ colors may provide useful selection methods for high redshift ULIRGs. The $B-R$ vs $R-L15$ colors plotted in figure 4 show that there is indeed a significant redder population of AKARI sources with $R-L15>4$ that cannot be explained by the colors of normal quiescent galaxies or low-redshift star-forming galaxies. For these sources with 15 μm AB magnitudes of 18, 19, this corresponds to R magnitudes of >22, >23 respectively.

For the AKARI 15μm sources with successful identifications in the Subaru/Suprime-cam source catalog, we find approximately 60 (40)% of the population with $R-L15>4$ (5). There is also a significant fraction of the population (25%) with very red colors of $R-L15>6$. It is noteworthy that the sources detected in the ISOCAM deep surveys in the HDF-S (Oliver et al. 2002; Mann et al. 2002) show mostly bluer ($R-L15<5$) colors, except for two sources, perhaps due to its shallower depth. These red sources populate the color–color parameter space occupied by the model SED templates for high redshift ULIRGs in figure 4. Note that Rowan-Robinson et al. (2004) found that around $\sim$ 14% of the sources in the ELAIS final band merged catalogue ($S_{15\mu m}>0.7$ mJy) could be attributed to ULIRGs. Given the deeper nature of the AKARI NEP survey, we may expect a significantly larger fraction of ULIRGs in our sample that most probably populate the $R-L15>6$ region of the $B-R$ vs $R-L15$ color–color plane. This interpretation is also supported by the evolving mid-infrared luminosity function recently derived based on the Spitzer 24 μm deep surveys (Le Floc'h et al. 2005; Pérez-González

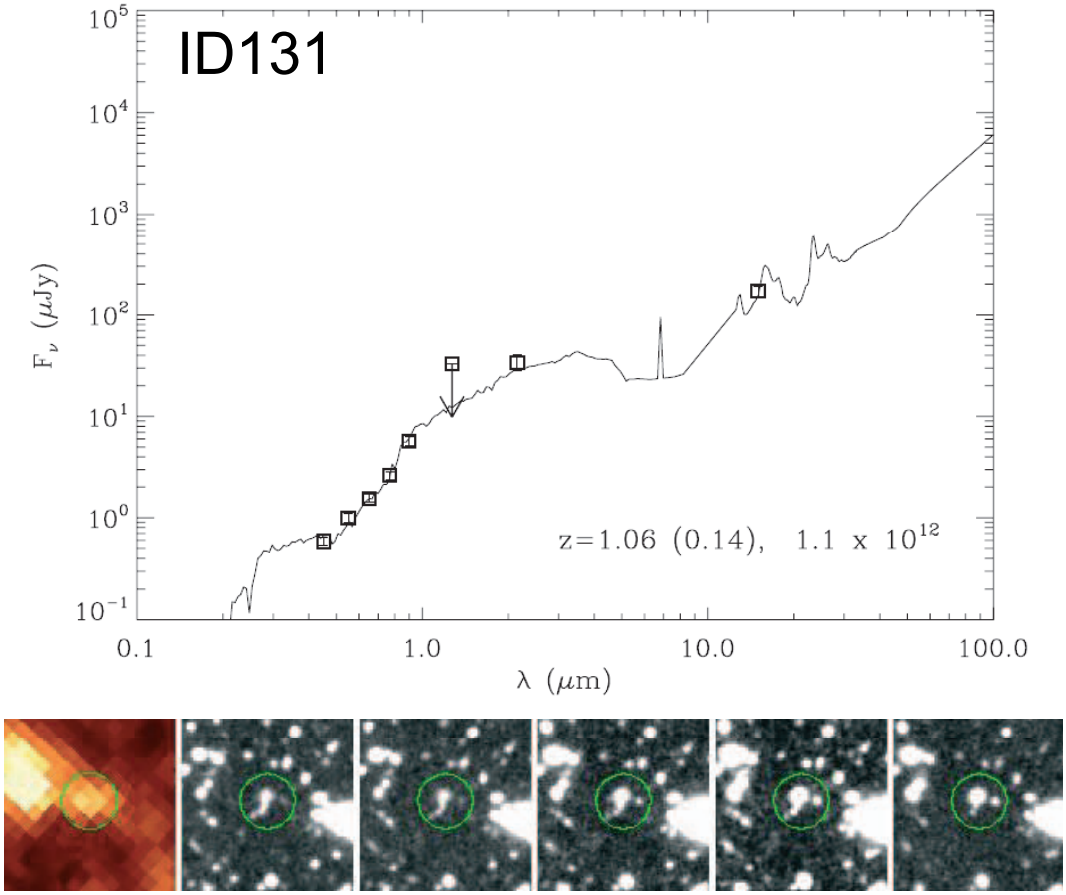

Fig. 8. Example of the SED fitting (top) and the postage stamp images (bottom, *L15*, B, V, R, i', and z' from left to right) for sources with secure K_s photometric data, in the case of ID 131. The radius of the circles in all the postage stamps is 5″.

et al. 2005). Although we do not show the track for the AGN template SED, it should be noted that the power-law SEDs of dusty obscured AGN can satisfy $R-L15 > 5$ for the power-law index $\alpha < -1.5$ ($f_\nu \propto \nu^\alpha$). Alonso-Herrero et al. (2005) present a sample of such AGN SEDs from $\alpha = -0.5$ down to $\alpha = -2.8$. Thus, it is likely that a fraction of our 15μm sources may in fact be highly obscured AGN.

So far the spectroscopic redshifts for the red 15 μm sources are not available, and it is not easy to estimate their physical quantities, such as infrared luminosities, and stellar masses. However, for near-future follow-up studies, it is valuable to present a crude picture of the sources via optical colors. Figure 7 shows a $B-R$ vs $R-z'$ plot for the 15 μm sources with $R-L15 > 5$, compared with the SED templates of the starburst (M 82), ULIRGs (Arp 220, HR 10). The red 15 μm sources are distributed widely over the color parameter space, but at least we can say that the colors can be explained by SED templates with $z \leq 2$. Of corse the SED templates presented here are not unique, and there exists a wide variety of SED shapes for starburst galaxies (see also Takagi et al. 2007). Thus, optical and near-infrared spectroscopic follow-ups with ground-based telescopes are essential to understand the nature of these red 15 μm sources.

3.2. *Nature of the Selected 15 μm Sources*

If the 15 μm sources are located at $z \geq 1$, quantitative studies of the 15 μm sources require near-infrared (J and K_s-band) photometry, since the Balmer or 4000 A break of the galaxy's SED is redshifted beyond optical wavelengths. For example, we may classify the 15 μm sources into either Extremely Red Objects (Mannucci et al. 2002; Miyazaki et al. 2003) or BzKs (Daddi et al. 2004) based on their color–color criteria. Unfortunately, the K_s-band data available so far is found to be too shallow to extract the BzK population at a high redshift ($1.4 < z < 2.5$, Daddi et al. 2004). However, we found six sources satisfying the ERO criterion ($R - K_s > 3$ in AB magnitude), and thus we attempted SED fittings of these sources in order to estimate their photometric redshifts, infrared luminosities, and SED types.

We fitted the observed SEDs using the Bayesian photometric redshift code of Benítez (2000). For the SED templates to compare with the data, we adopted 100 SEDs of IR luminous galaxies from Chary and Elbaz (2001). These SEDs were modified by applying galactic extinction corrections of $E(B-V) = 0.041$, estimated from the far-infrared brightness of the NEP (Schlegel et al. 1998) using an extinction curve of Calzetti et al. (2000). After fitting, we obtained an estimate of the

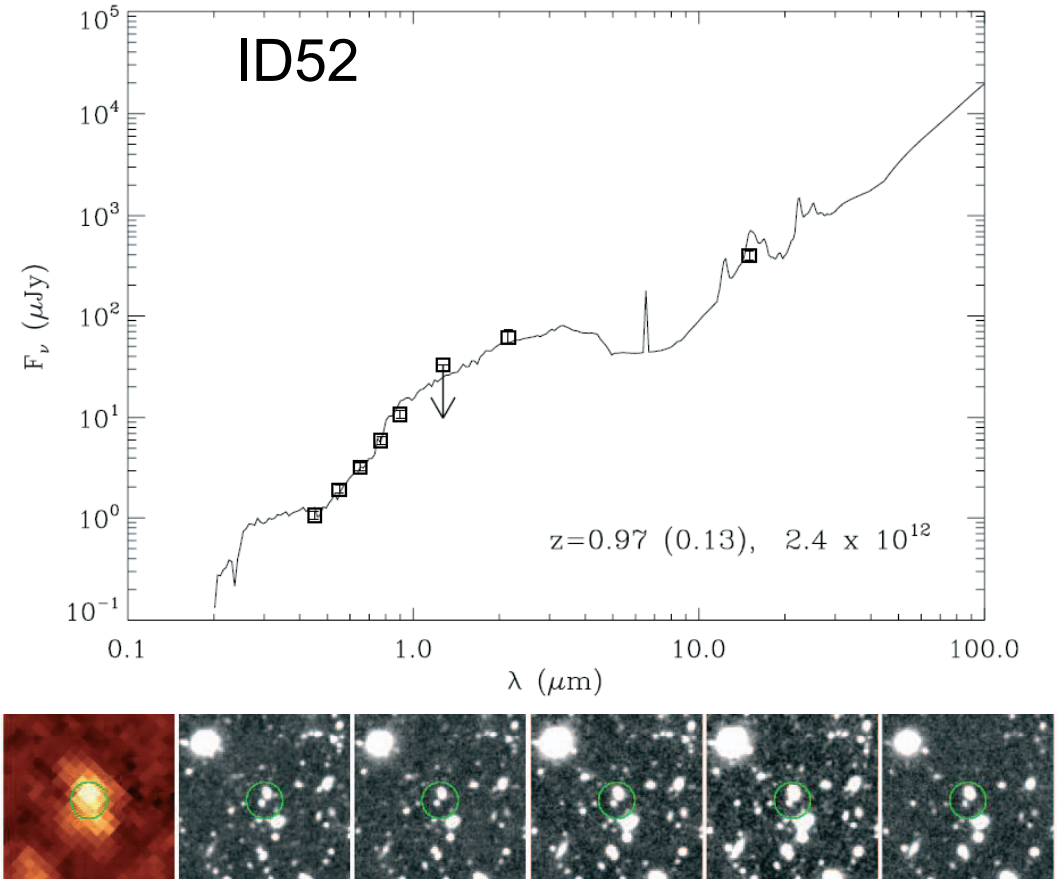

Fig. 9. Example of the SED fitting (top) and the postage stamp images (bottom), in the case of ID 52. See figure 8 caption for an explanation of the figures.

photometric redshift as well as the best-fit SED template. The infrared luminosity was calculated by integrating the fluxes beyond the rest-frame 5 μm of the best-fit SED template. We found that the formal errors in the photometric redshifts from the fitting program are under 20%, and the uncertainty in the IR luminosity to be on the order of at least a factor of a few. The estimates, however, might have a larger uncertainty if an object has a more complex SED than a simple, single-component SED, as demonstrated for the object ID 151 described below. We expect that these uncertainties will be reduced when we have data between the J-band and the 15 μm, and also at 24 μm at the end of the NEP survey.

3.2.1. Dusty starburst candidates

Among the six 15 μm sources satisfying the ERO criterion, two sources (ID 131 and ID 52) can be fitted well with $z \sim 1$ dusty starburst templates. In figures 8 and 9, the results are shown: for ID 131, the SED fitting gives a photometric redshift ($z_{\rm phot}$) of 1.06 ± 0.14, and total infrared luminosity ($L_{\rm IR}$) of $1.1 \times 10^{12}\,L_{\odot}$, while for ID 52, $z_{\rm phot} = 0.97 \pm 0.13$, $L_{\rm IR} = 2.4 \times 10^{12}\,L_{\odot}$.

3.2.2. E/S0 plus dusty starburst composites?

The optical – $K_{\rm s}$-band SEDs of the final four 15 μm sources satisfying the ERO criterion can be fitted well by not only the dusty starburst templates at $z = 0.47$ (figure 10 top), but also by old E/S0 like SEDs. However, for the latter case the 15 μm fluxes originating from the circumstellar dust of the AGB stars seems to be too weak to explain the observed fluxes. Therefore, we propose that the SEDs can be explained by a composite SED of the E/S0-like stellar population plus the dusty starburst population. As shown in figure 10, middle, the SED of ID 151 can be fitted by 0.8 Gyr-old [after a burst of star-formation over 0.1 Gyr produced by the 1996 version of Bruzual & Charlot (1993) models] stellar population and a dusty starburst with $L_{\rm IR} = 10^{12} L_{\odot}$, which contributes 20% of the $K_{\rm s}$-band flux. In this case we obtain $z_{\rm phot} = 1.47 \pm 0.10$. At the moment, both fits seem to be acceptable. Measurements in the intermediate bands (3–11 μm) soon available from the AKARI "NEP-Deep" survey will help to break this degeneracy.

The AKARI NEP survey (Matsuhara et al. 2006) is continuing and will achieve comparable mid-infrared depths to those described in this paper, over nine bands between 2 and 24 μm. Since the "NEP-Deep" field covers approximately a 20-times larger area than the performance verification field, we can expect to discover about 2000 faint ($\leq 100\,\mu$Jy) sources, from which we can construct statistically meaningful, optical – mid-infrared SED samples to further understand the nature of the 15 μm population introduced in this paper.

4. Summary

The results of optical identifications are presented for 257 15 μm sources detected with a deep 15 μm survey over

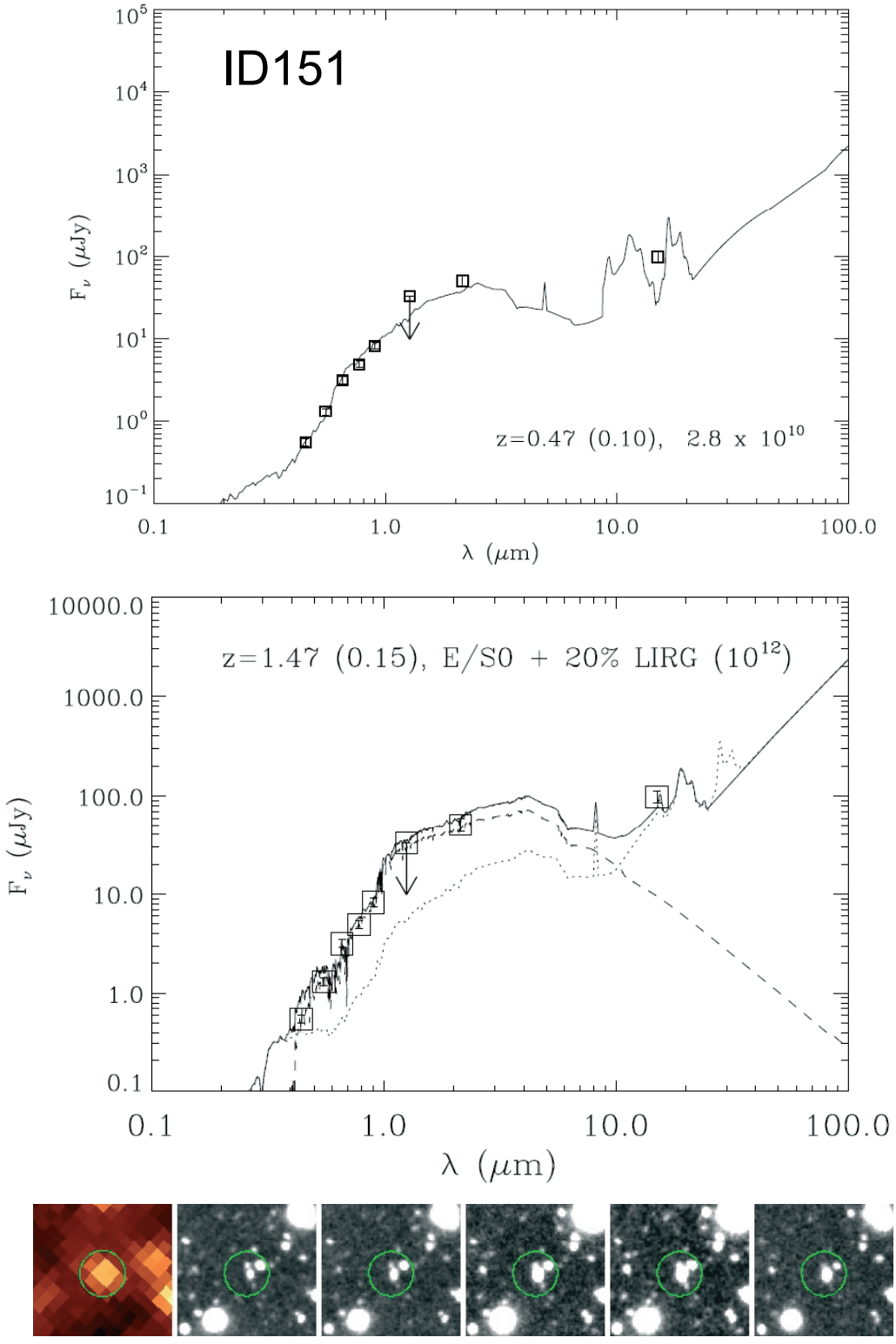

Fig. 10. Example of the SED fitting (top two panels) and the postage stamp images (bottom) for sources which can be fitted with not only by the dusty starburst templates, but also by composites of E/S0 and dusty starburst SEDs. See figure 8 caption for explanations of figures.

approximately 80 arcmin^2 area in the AKARI performance verification field around the North Ecliptic Pole. In comparison with the previous 15 μm surveys with ISO/ISOCAM and the Spitzer/IRS peak-up imaging, the AKARI 15 μm sample is particularily unique in its faint flux limit ($\sim$ 40 μJy) : the 15 μm fluxes of approximately a half of the sample are below 100 μJy. Optical counterparts were searched for within a 2″–3″ search radius in both a $BVRi'z'$ catalog generated from the deep Subaru/Suprime-cam field, which covers one-third of the performance verification field, and the $g'r'i'z'$ catalog, based on a wide-area survey made with MegaCam at CFHT. We found that the $B-R$ and $R-z'$ colors of sources with successful optical identifications are systematically redder than that of the entire optical sample in the same field, indicating that the 15 μm sources may be located at relatively high redshifts. Moreover, approximately 40% of the 15 μm sources show colors $R-L15 > 5$, which cannot be explained by the SED of normal quiscent spiral galaxies, but is consistent with the SEDs of redshifted ($z > 1$) starburst or ULIRGs. This result indicates that the fraction of ULIRGs in the faint 15 μm sample is much larger than that in the brighter 15 μm sample. Based on optical to 15 μm SED fittings for a few sources with the K_s-band data available so far, we found that several 15 μm sources can be explained by an SED of the dusty starburst population (ULIRGs). Deep J and K_s-band data as well as AKARI mid-infrared multi-band data other than 15 μm are essential to further constrain the nature of the faint 15 μm population.

This work is partly based on observations with AKARI, a JAXA project with the participation of ESA. A part of optical observations is based on observations obtained with MegaPrime/MegaCam, a joint project of CFHT and CEA/DAPNIA, at the Canada-France-Hawaii Telescope (CFHT) which is operated by the National Research Council (NRC) of Canada, the Institute National des Sciences de l'Univers of the Centre National de la Recherche Scientifique of France, and the University of Hawaii. We would like to thank all AKARI team members for their support on this project. The Korean participation to AKARI Project was supported by the KRF Grant No. R14-2002-01000-0 and BK21 program to SNU. M.I. and E.K. were supported by the Korea Science and Engineering Foundation (KOSEF) grant funded by the Korea government (MOST), No. R01-2005-000-10610-0. T. Takagi is supported by a Japan Society for the Promotion of Science (JSPS) Fellowship for Research. H.M.L and M.G.L. were supported in part by ABRL (R14-2002-058-01000-0). This work is partly supported by the JSPS grants (grant numbers 15204013, and 16204013).

References

Alonso-Herrero, A., et al. 2006, ApJ, 640, 167
Aussel, H., Casarsky, C. J., Elbag, D., & Starck, J. L. 1999, A&A, 342, 313
Benítez, N. 2000, ApJ, 536, 571
Bertin, E., & Arnouts, S. 1996, A&AS, 117, 393
Bruzual, A. G., & Charlot, S. 1993, ApJ, 405, 538
Calzetti, D., Armus, L., Bohlin, R. C., Kinney, A.L., Koornneef, J., & Storchi-Bergmann, T. 2000, ApJ, 533, 682
Caputi, K. I., et al. 2006, ApJ, 637, 727
Chary, R. 2006, astro-ph/0612736
Chary, R., & Elbaz, D. 2001, ApJ, 556, 562
Daddi, E., Cimatti, A., Renzini, A., Fontana, A., Mignoli, M., Pozzetti, L., Tozzi, P., & Zamorani, G. 2004, ApJ, 617, 746
Efstathiou, A., & Rowan-Robinson, M. 2003, MNRAS, 343, 322
Efstathiou, A., Rowan-Robinson, M., & Siebenmorgen, R. 2000, MNRAS, 313, 734
Elbaz, D., Cesarsky, C. J., Chanial, P., Aussel, H., Franceschini, A., Fadda, D., & Charry, R.-R. 2002, A&A, 384, 848
Fazio, G. G., et al. 2004, ApJS, 154, 10
Franceschini, A., et al. 2003, A&A, 403, 501
Genzel, R., & Cesarsky, C. J. 2000, ARA&A, 38, 761
Graham, J. R., & Dey, A. 1996, ApJ, 471, 720
Gruppioni, C., Lari, C., Paggi, F., Zamorani, G., Franceschini, A., Oliver, S., Rowan-Robinson, M., & Serjeant, S. 2002, MNRAS, 335, 831
Houck, J. R., et al. 2004, ApJS, 154, 18
Hwang, N., et al. 2007, ApJS in press
Imai, K., Matsuhara, H., Oyabu, S., Wada, T., Takagi,T., Fujishiro, N., Hanami, H., & Pearson, C. P. 2007, AJ, 133, 2418
Le Floc'h, E., et al. 2005, ApJ, 632, 169
Mann, R. G., et al. 2002, MNRAS, 332, 549
Manners, J. C., et al. 2004, MNRAS, 355, 97
Mannucci, F., et al. 2002, MNRAS, 329, L57
Matsuhara, H., et al. 2006, PASJ, 58, 673
Matsuhara, H., Shibai, H., Onaka, T., & Usui, F. 2005, Adv. Space Res., 36, 1091
Miyazaki, M., et al. 2003, PASJ, 55, 1079
Murakami, H., et al. 2007, PASJ, 59, S369
Oliver, S., et al. 2002, MNRAS, 332, 536
Onaka, T., et al. 2007, PASJ, 59, S401
Papovich, C., et al. 2004, ApJS, 154, 70
Pearson, C. P. 2005, MNRAS, 358, 1417
Pérez-González, P. G., et al. 2005, ApJ, 630, 82
Rieke, G. H., et al. 2004, ApJS, 154, 25
Rowan-Robinson, M., et al. 2004, MNRAS, 351, 1290
Schlegel, D. J., Finkbeiner, D. P., & Davis, M. 1998, ApJ, 500, 525
Serjeant, S., et al. 2000, MNRAS, 316, 768
Takagi, T., Arimoto, N., & Hanami, H. 2003a, MNRAS, 340, 813
Takagi, T., Vansevičius, V., & Arimoto, N. 2003b, PASJ, 55, 385
Teplitz, H. I., Charmandaris, V., Chary, R., Colbert, J.,W., Armus, L., & Weedman, D. 2005, ApJ, 634, 128
Teplitz, H. I., Chary, R., Colbert, J. W., Siana, B., Elbaz, D., Dickinson, M., & Papovich, C. 2006, BAAS, 38, 1079
Wada, T., et al. 2007, PASJ, 59, S515
Werner, M. W., et al. 2004, ApJS, 154, 1